°C; IR (KBr, cm^{-1}) 3545, 3470, 3300, 1475, 1460, 1370, 1300, 1220, 1175, 1050, 1040, 935, 830, 750, 650; ^1H NMR (300 MHz, CD_3CN) δ 6.65 (t, J = 2.1 Hz, 2 H), 3.83 (t, J = 2.1 Hz, 2 H), 3.42 (br s, 2 H), 3.03 (m, 1 H), 1.58 (s, 3 H); ^{13}C NMR (75 MHz, CD_3CN) ppm 139.18, 113.31, 113.22, 66.61, 66.47, 60.73, 46.93, 19.21. Anal. Calcd for $C_{13}H_{10}N_4O$: C, 65.54; H, 4.23. Found: C, 65.40; H, 4.36.

For **27**: ^1H NMR (300 MHz, acetone-d_6) δ 6.79 (t, J = 2.1 Hz, 2 H), 4.14 (t, J = 2.1 Hz, 2 H), 3.61 (s, 2 H), 2.86 (br s, 1 H), 1.29 (s, 3 H).

Cycloaddition of (*Z*)-1,2-Bis(phenylsulfonyl)ethylene to 6. A solution of **6** (100 mg, 9.09×10^{-4} mol) and the disulfone (841 mg, 2.73 mmol) in 1.5 mL of dichloromethane was maintained at 90000 psi and room temperature for 2 days. Solvent removal left a white solid (86%), ^1H NMR analysis of which (300 MHz) showed **28** and **29** to be present in a 4.55:1 ratio. Repeated recrystallization of this material from dichloromethane–methanol provided pure **28** as colorless crystals: mp 299–300 °C; IR (KBr, cm^{-1}) 3505, 1445, 1365, 1335, 1295, 1270, 1185, 1160, 1145, 1085, 1040, 765, 735, 720, 695, 610; ^1H NMR (300 MHz, DMSO-d_6) δ 7.99–7.96 (m, 4 H), 7.76–7.73 (m, 6 H), 6.33 (t, J = 1.6 Hz, 2 H), 4.55 (s, 2 H), 4.33 (t, J = 5.5 Hz, 1 H), 3.15 (d, J = 5.5 Hz, 2 H), 2.49 (m, 2 H), 0.86 (s, 3 H); ^{13}C NMR (75 MHz, DMSO-d_6) ppm 141.28, 133.51, 133.22, 129.12, 128.14, 69.61, 62.55, 61.77, 53.48, 16.66; MS m/z ($M^+ - SO_2C_6H_5$) calcd 277.0898, obsd 277.0968. Anal. Calcd for $C_{21}H_{22}O_5S_2$: C, 60.27; H, 5.30. Found: C, 59.87; H, 5.42.

For **29**: ^1H NMR (300 MHz, DMSO-d_6) δ 7.98–7.80 (m, 4 H), 7.76–7.63 (m, 6 H), 6.39 (m, 2 H), 4.55 (m, 2 H), 4.33 (t, J = 5.2 Hz, 1 H), 3.15 (d, J = 5.2 Hz, 2 H), 2.58 (m, 2 H), 0.80 (s, 3 H); ^{13}C NMR (75 MHz, DMSO-d_6) ppm 141.34, 134.54, 133.77, 129.51, 127.82, 69.35, 62.69, 61.28, 52.76, 16.09.

Acknowledgment. We thank the National Institutes of Health for their support of this research program through Grant CA-12115.

Supplementary Material Available: Tables of bond distances and angles, least-squares planes, final fractional coordinates, and thermal parameters for **17** and **22** (11 pages); observed and calculated structure factors for **17** and **22** (6 pages). Ordering information can be found on any current masthead page.

Binuclear Electron Reservoir Complexes:[1] Syntheses, Reactivity, and Electronic Structure of the 37- and 38-Electron Fulvalene Complexes $(Fe_2(\mu_2,\eta^{10}\text{-}C_{10}H_8)(arene)_2)^{n+}$, n = 0, 1

Marie-Hélène Desbois,[†] Didier Astruc,*[,†] Jacques Guillin,[§,‡] François Varret,[§] Alfred X. Trautwein,[‡] and Gérard Villeneuve[⊥]

Contribution from the Laboratoire de Chimie Organique et Organométallique, U.A. CNRS n° 35, Université de Bordeaux I, 351 Cours de la Libération, 33405 Talence Cédex, France, Groupe de Physique et Chimie du Solide, U.A. CNRS n° 807, Université du Maine, 72017 Le Mans Cédex, France, Institut für Physik, Medizinische Universität zu Lübeck, Ratzeburger Allee 160, 2400 Lübeck, R.F.A., Laboratoire de Chimie du Solide du CNRS, Université de Bordeaux I, 351 Cours de la Libération, 33405 Talence Cédex, France. *Received July 27, 1988*

Abstract: One-electron reduction of the dications $(Fe_2Fv(Ar)_2)^{2+}$ **2–8** in THF with Na/Hg gives high yields of the 37e⁻ Fe^IFe^{II} mixed-valence complexes **9–15**. The C_6Me_6 complex $(Fe_2Fv(HMB)_2)^+PF_6^-$, **9**, is thermally stable at 20 °C, whereas analogues with other arene ligands are not and need be isolated at lower temperatures. The symmetrical, purple complexes **9–15** show three g values around 2 by ESR spectroscopy at 77 or 4.2 K as Fe^I monomers. Mössbauer spectra of **9** and of $(Fe_2Fv(C_6H_6)_2)^+PF_6^-$, **10**, show only one quadrupole doublet at 293, 77, and 4.2 K, the parameters of which are not temperature dependent, unlike those of the Jahn–Teller active Fe^I monomers and of the localized Fe^IFe^{II} mixed-valence complexes. In addition, Mössbauer spectra, under external applied magnetic field, show the presence of only one electron for the "Fe_2" unit. Thus, the mixed-valence complexes $(Fe_2Fv(arene)_2)^+$ are delocalized on the Mössbauer time scale (10^7 s^{-1}). EHT and SCC-Xα calculations were performed and compared for both the monomeric Fe^I and the dimeric Fe^IFe^{II} and Fe^IFe^I complexes. A good agreement was found with Mössbauer parameters. The MO diagram of the 37e⁻ species shows a large HOMO–LUMO gap as expected from the non-variation of the quadrupole splitting values with the temperature. Two-electron reductions of **2**, **3**, and **8** in THF also using Na/Hg give the green organometallic 38e⁻ biradicals $Fe_2Fv(C_6R_6)_2$ (R = Me, **16**; R = H, **17**; R = Et, **22**). Jahn–Teller active Fe^I units are observed by Mössbauer spectroscopy in high-temperature phase. An antiferromagnetic transition occurs at 37 K, for **16**, as indicated by the Mössbauer and magnetic susceptibility data. The magnetic coupling of **16** at low temperature may be facilitated by the steric effect of the methyl substituents on the rotation around the C–C bond.

Among the various organometallic and inorganic families disclosing several stable oxidation states,[2] mononuclear organoiron "electron reservoir" complexes[3] have proved useful because of the simplicity of their large scale preparation,[4] the possibilities of functionalization,[5] and their efficient stoichiometric[6] as well as catalytic electron-transfer processes.[7,8] However, the number of available oxidation states is limited in mononuclear frameworks. The redox series is richer in binuclear species, specially if mixed-valence states are accessible. For instance, nature uses binuclear ferredoxins[9] (Fe_2S_2) as redox catalysts in the respiratory chain. To what extent the fulvalene bridge brings about satisfactory delocalization can be understood from the interaction and mutual

[†] Laboratoire de Chimie Organique et Organométallique, Université de Bordeaux I.
[§] Laboratoire de Physique et Chimie du Solide, Université du Mans.
[‡] Institüt fur Physik, Medizinische Universität zu Lübeck.
[⊥] Laboratoire de Chimie du Solide du CNRS, Université de Bordeaux I.

(1) (a) Preliminary synthetic studies were effected in the Laboratoire de Chimie des Organométalliques, University of Rennes I. (b) *Organometallic Electron Reservoirs*; part 36. For part 35 see: Desbois, M.-H.; Astruc, D.; Guillin, J.; Varret, F. *Organometallics*, in press. Part 34 reports the syntheses and electrochemistry of the 36e⁻ precursors: *Organometallics*, in press. (c) This paper overlaps with parts of the third cycle theses of M.-H.D. and J.G. Desbois, M.-H.; Astruc, D.

(2) (a) Connelly, N. G.; Geiger, W. E. *Adv. Organomet. Chem.* **1984**, *23*, 1. (b) Geiger, W. E.; Connelly, N. G. *Ibid.* **1985**, *24*, 87. (c) Dessy, R. E.; Bares, L. A. *Acc. Chem. Res.* **1972**, *5*, 415. (d) de Montauzon, D.; Poilblanc, R.; Lemoine, P.; Gross, M. *Electrochim. Acta* **1978**, *23*, 1247. (e) Denisovitch, L. I.; Gubin, S. P. *Russ. Chem. Rev. Engl.* **1977**, *46*, 27. (f) Chu, C. T.-W.; Lo, F. Y.-K.; Dahl, L. F. *J. Am. Chem. Soc.* **1982**, *104*, 3409. (g) Kochi, J. K. *Organometallic Mechanisms and Catalysis*; Academic Press: New York, 1978.

0002-7863/89/1511-5800$01.50/0

influence between both redox centers. It has long been known that the biferrocene cation is a localized mixed-valence complex[10] on the Mössbauer time scale, whereas the biferrocenylene cation is delocalized.[11] Recently, Hendrickson has shown the influence of the counteranion on the localization of the mixed-valence in disubstituted biferrocene cations.[12] We have studied the reduced states of two isomers A and B including the nature of the mix-

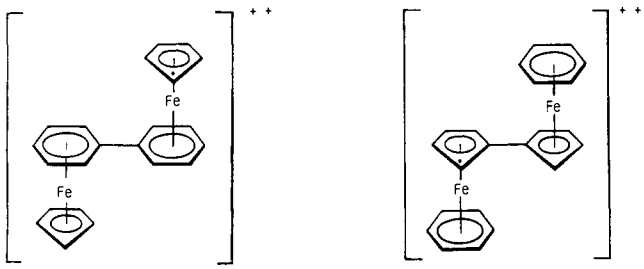

ed-valence derivatives and of the coupling in the direduced species. The $2e^-$ reduction of A and the electron-transfer chemistry of the C_5Me_5 analogue are detailed in a forthcoming paper.[13a,b]

In a preliminary communication,[13c] we have reported a new redox series of fulvalene diiron sandwiches which is synthetically accessible from biferrocene: the symmetric series (B, C) in which

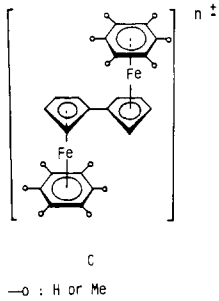

two $FeCp(C_6R_6)$ units (R = H, Me, Et) are linked. In this article, we are reporting full details of synthesis, reactivity, and electronic structure of the $37e^-$ and $38e^-$ states of this series including SCC-Xα molecular orbitals calculations; meanwhile we pose the problem of the delocalization in the Fe^IFe^{II} species and of the coupling in the Fe^IFe^I complexes. (See ref 1b for the $36e^-$ precursors.)

Experimental Section

General Data. Reagent grade tetrahydrofuran (THF), 1,2-dimethoxyethane (DME), diethyl ether (Et_2O), and pentane were predried on Na foil and distilled from sodium benzophenone ketyl under argon just before use. Benzene, toluene, heptane, and decahydronaphthalene were treated identically and stored under argon. Acetonitrile was stirred under argon overnight on phosphorus pentoxide, distilled from sodium carbonate, and stored under argon. Methylene chloride was distilled from calcium hydride just before use. All other chemicals were used as received. All manipulations were done by Schlenk technique or in a nitrogen-filled Vacuum Atmosphere drylab. Infrared spectra were recorded with Pye-Unicam SP 1100 and Perkin-Elmer 1420 ratio recording infrared spectrophotometers which were calibrated with polystyrene. Samples were examined in solution (0.1-mm cells with NaCl windows) or between NaCl disks in Nujol. Electronic spectra (visible and near infrared) were recorded between −50 °C and +25 °C with Cary 14 and Cary 219 spectrophotometers with 10-mm quartz cells. ESR spectra were recorded using a Brücker ER 200tt X band (Bordeaux) and a Varian E 112 (Grenoble) spectrometer. Mössbauer spectra were recorded with a 25-m Ci ^{57}Co source on Rh, by using a symmetric triangular sweep mode (Le Mans). Elemental analyses were performed by the Center of Microanalyses of the CNRS (Lyon-Villeurbanne). Variable temperature (1.9–266 K) magnetic susceptibilities were recorded at 0.1 T with a SQUID SHE magnetometer associated with a supraconductor magnet; dc conductivity measurements were done in a home-built cell monitored by microcomputer (Bordeaux).

Preparations. The following abbreviations will be used for the ligand formula: η^5-C_5H_5 = Cp; μ_2,η^{10}-$C_{10}H_8$ = Fv; η^6-C_6Me_6 = HMB; η^6-C_6H_6 = Bz; η^6-1,3,5-$C_6H_3Me_3$ = Mes; η^6-C_6H_5Me = Tol; η^6-$C_6H_5CH_2CH_3$ = EtBz.

1. $(Fe_2Fv(HMB)_2)^+PF_6^-$ (9). A 1.81-g sample of $(Fe_2Fv(HMB)_2)^{2+}(PF_6^-)_2$ (2 mmol) in 50 mL of DME is stirred with 48.7 g of Na/Hg amalgam (1%, 10 mmol) for 2 h at room temperature under argon. A purple suspension is observed. DME is then removed in "vacuo", and the purple crude product is washed three times with 20 mL of THF in order to remove the $Na^+PF_6^-$ salt. The residue is then rapidly extracted with acetone, precipitated with Et_2O, and recrystallized from acetone. Standing overnight at −40 °C affords a purple microcrystalline, air-sensitive powder of $(Fe_2Fv(HMB)_2)^+PF_6^-$ (1.202 g, 80% yields): visible (THF, 20 °C) λ = 554 nm (ϵ = 7660 L mol^{-1} cm^{-1}); magnetic susceptibility (Gouy method, μ = 1.7 μ_B); ESR, see Table I for results. Anal. Calcd for $C_{34}H_{44}Fe_2PF_6$: C, 57.54; H, 6.20; Fe, 15.79; P, 4.37. Found: C, 57.98; H, 6.27; Fe, 15.75; P, 4.36.

2. Reduction of $(Fe_2Fv(HMB)_2)^{2+}(PF_6^-)_2$ Using $LiAlH_4$. A 0.1-g sample of this dication (0.117 mmol) is stirred in 10 mL of THF with 0.445 g of $LiAlH_4$ (11.7 mmol) at −80 °C under argon. The system immediately turns purple at this temperature with formation of the Fe^IFe^{II} complex. Further reduction to Fe^IFe^I complex never occurs even after 8 h reaction times at −80 °C. Increasing the temperature up to −50 °C leads to the hydrogenated diamagnetic product. The purple complex obtained is identified as $(Fe_2Fv(HMB)_2)^+PF_6^-$ by comparison with an authentic sample.

3. Reduction of $(Fe_2Fv(HMB)_2)^{2+}(PF_6^-)_2$ Using FeCp(HMB) (25). A 0.1-g sample of the dication (0.117 mmol) is stirred in 10 mL of THF with 0.033 g of FeCp(HMB)[4] (0.117 mmol) at room temperature under argon. The green solution of monomeric Fe^I immediately reacts and gives a purple precipitate of $(Fe_2Fv(HMB)_2)^+PF_6^-$ characterized by comparison with an authentic sample.

4. $(Fe_2Fv(Bz)_2)^+PF_6^-$ (10). A 0.4-g sample of the dication (0.583 mmol) is stirred in 20 mL of THF with 6.70 g of Na/Hg amalgam (1%, 2.915 mmol) for 1 h at −20 °C under argon. The purple precipitate obtained is filtered in another Schlenk tube at −80 °C and washed three more times with 20 mL of THF at −20 °C. The residue is then rapidly extracted with a minimum of acetone at −20 °C. Cold Et_2O is then added, and the mixture is again cooled down to −80 °C, which provides 0.249 g of purple microcrystalline $(Fe_2Fv(Bz)_2)^+PF_6^-$. Fast transfer of this thermally unstable cation to a Mössbauer cell under a cold stream of argon (−10 °C) affords the observation of a pure Mössbauer doublet: see Table II for results; visible (THF, −20 °C) λ = 552 nm (ϵ = 1100 L mol^{-1} cm^{-1}).

$(Fe_2Fv(Bz)_2)^{2+}(PF_6^-)_2$ also undergoes a monoelectronic reduction in presence of 100 equiv excess of $LiAlH_4$. Procedure 2 was applied and

(3) (a) Astruc, D. *Acc. Chem. Res.* **1986**, *12*, 377. (b) Astruc, D. *Comments Inorg. Chem.* **1987**, *6*, 61.
(4) Astruc, D.; Hamon, J.-R.; Lacoste, M.; Desbois, M.-H.; Madonik, A. M.; Roman, E. *Organometallic Synthesis*; **1988**, *4*, 172.
(5) (a) Román, E.; Dabard, D.; Moinet, C.; Astruc, D. *Tetrahedron Lett.* **1979**, *16*, 1433. (b) Guerchais, V.; Astruc, D. *J. Chem. Soc., Chem. Commun.* **1984**, 881. (c) Guerchais, V.; Román, E.; Astruc, D. *Organometallics* **1986**, *5*, 2505.
(6) (a) Desbois, M.-H.; Michaud, P.; Astruc, D. *J. Chem. Soc., Chem. Commun.* **1985**, 450. (b) Michaud, P.; Lapinte, C.; Astruc, D. *Annals New York Acad. Sci.* **1983**, 97.
(7) Buet, A.; Darchen, A.; Moinet, C. *J. Chem. Soc., Chem. Commun.* **1979**, 447.
(8) Astruc, D. *Angew. Chem., Int. Ed. Engl.* **1988**, *27*, 643.
(9) (a) Holm, R. H. In *Biological Aspects of Inorganic Chemistry*; Addison, A. W., Cullen, W. R., Dolphin, D., James, B. R., Eds.; Wiley: New York, 1977; pp 71–112. (b) Holm, R. H. *Acc. Chem. Res.* **1977**, *10*, 427.
(10) (a) Morrison, W. H.; Hendrickson, D. N. *J. Chem. Phys.* **1973**, *59*, 380. (b) Cowan, D. O.; Collins, R. L.; Kaufman, F. *J. Phys. Chem.* **1971**, *75*, 2025. (c) Morrison, W. H.; Krogsud, S.; Hendrickson, D. N. *Inorg. Chem.* **1973**, *12*, 1998. (d) Cowan, D. O.; Candela, G. A.; Kaufman, F. *J. Am. Chem. Soc.* **1971**, *93*, 3889. (e) Kaufman, F.; Cowan, D. O. *Ibid.* **1970**, *92*, 6198. (f) Cowan, D. O.; Park, J.; Barber, M.; Swift, P. *J. Chem. Soc., Chem. Commun.* **1971**, 1444. (g) Cowan, D. O.; Levanda, C.; Park, J.; Kaufman, F. *Acc. Chem. Res.* **1973**, *6*, 1. (h) Rudie, A. W.; Davison, A.; Frankel, R. B. *J. Am. Chem. Soc.* **1979**, *101*, 1629. (i) Morrison, W. H.; Hendrickson, D. N. *Inorg. Chem.* **1975**, *14*, 2331. (j) Iijima, S.; Saida, R.; Motoyama, I.; Sano, H. *Bull. Chem. Soc. Jpn.* **1981**, *54*, 1375. (k) Motoyama, I.; Suto, K.; Katada, M.; Sano, H. *Chem. Lett.* **1983**, 1215.
(11) For a recent, comprehensive review, see: Mueller-Westerhoff, U. T. *Angew. Chem., Int. Ed. Engl.* **1986**, *25*, 702.
(12) (a) Hendrickson, D. N.; Oh, S. M.; Dong, T.-Y.; Moore, M. F. *Comments Inorg. Chem.* **1985**, *4*, 329 and references cited therein. (b) Dong, T. Y.; Hendrickson, D. N.; Pierpont, C. G.; Moore, M. F. *J. Am. Chem. Soc.* **1986**, *108*, 963. (c) Dong, T. Y.; Kambara, T.; Hendrickson, D. N. *J. Am. Chem. Soc.* **1986**, *108*, 4423. (d) Dong, T. Y.; Hendrickson, D. N.; Iwai, K.; Cohn, M. J.; Geib, S. J.; Rheingold, A. L.; Sano, H.; Motoyama, I.; Nakashima, S. *J. Am. Chem. Soc.* **1985**, *107*, 7996.
(13) (a) Lacoste, M.; Toupet, L.; Varret, F.; Astruc, D., submitted for publication (see also ref 13b). (b) Lacoste, M.; Varret, F.; Toupet, L.; Astruc, D. *J. Am. Chem. Soc.* **1987**, *109*, 6504. (c) Desbois, M.-H.; Astruc, D.; Guillin, J.; Mariot, J.-P.; Varret, F. *J. Am. Chem. Soc.* **1985**, *107*, 5280.

Table I. ESR Spectroscopic Results for $Fe^{II}Fe^{I}$ and $Fe^{I}Fe^{I}$ Complexes in the Symmetrical Series[a]

$Fe_2Fv(Ar)_2$		g_x	g_y	g_z	g_1	g_2	μ (μ_B)
$(Bz)_2$	$Fe^{II}Fe^{I}$	2.0054	2.0726	1.9110			1.729
	$Fe^{I}Fe^{I}$				1.9947	2.0768	2.860
$(Tol)_2$	$Fe^{II}Fe^{I}$	1.9977	2.0645	1.9075			1.724
	$Fe^{I}Fe^{I}$				1.9798	2.0523	2.834
$(Mes)_2$	$Fe^{II}Fe^{I}$	1.9946	2.0666	1.9137			1.725
	$Fe^{I}Fe^{I}$				2.0096	2.0591	2.865
$(HMB)_2$[b]	$Fe^{II}Fe^{I}$	2.0055	2.0717	1.9060			1.728
	$Fe^{I}Fe^{I}$				2.0194	1.9209	2.810
HMB, Bz	$Fe^{II}Fe^{I}$	1.9596	2.0535	1.8569			1.728
	$Fe^{I}Fe^{I}$				2.0072	2.0626	2.865

[a] (THF, 3×10^{-4} mol/L, 77 K). $\mu = (^1/_3(g_x^2 + g_y^2 + g_z^2)(S+1)S)^{1/2}\mu_B$ where $S = ^1/_2$ for $Fe^{II}Fe^{I}$ and $S = 1$ for $Fe^{I}Fe^{I}$ systems. [b] A low intensity forbidden spin transition ($\Delta Ms = 2$) was observed at half field ($g = 4.2536$) for solid-state samples.

led to the purple complex $(Fe_2Fv(Bz)_2)^+PF_6^-$ identified by comparison with an authentic sample.

In the same way, $(Fe_2Fv(Bz)_2)^{2+}(PF_6^-)_2$ reacts at −20 °C with 1 equiv of FeCp(HMB) to give $(Fe_2Fv(Bz)_2)^+PF_6^-$.

5. $(Fe_2Fv(Tol)_2)^+PF_6^-$ (11). A 0.1-g sample of $(Fe_2Fv(Tol)_2)^{2+}(PF_6^-)_2$ (0.14 mmol) in 5 mL of THF is stirred with 0.53 g of $LiAlH_4$ (14 mmol) for 2 or 3 min at −80 °C under argon. The purple solution is then immediately transferred into an ESR tube at −80 °C: see Table I for results.

6. The same procedure as in 5 was used to obtain $(Fe_2Fv(Ar)_2)^+PF_6^-$ (Ar = EtBz (**12**); Mes (**13**); Bz, HMB (**14**)): see Table I for ESR results.

7. $Fe_2Fv(Bz)_2$ (17). A 0.8-g sample of the dication (1.166 mmol) is stirred in 20 mL of THF with 13.4 g of Na/Hg amalgam (1%, 4.830 mmol) for 4 h at −20 °C, under argon. THF is removed in "vacuo" from the deep green solution. The crude product was extracted twice with a minimum (30 mL) of cold toluene. Filtration and addition of 150 mL of cold pentane followed by cooling down to −80 °C provide dark green crystals (0.370 g, 0.933 mmol, 80%). Fast transfer to a Mössbauer cell under a stream of cold argon (−10 °C) affords the observation of Mössbauer spectra: see Table II for results; visible (THF, −50 °C); λ = 725 nm (ϵ = 1400 L mol^{-1} cm^{-1}).

8. $Fe_2Fv(HMB)_2$ (16). A 0.854-g sample of $(Fe_2Fv(HMB)_2)^{2+}(PF_6^-)_2$ (1 mmol) is stirred in 50 mL of THF with 23 g of Na/Hg amalgam (1%, 10 mmol at room temperature. The purple color of the monoreduced species first appears and is persistent for 2 h (reproducibility). After this time, the green $Fe^{I}Fe^{I}$ complex forms and immediately precipitates. Complete reduction is achieved in 4 h. This green complex is totally insoluble in all common solvents and extremely air sensitive: see Tables I and IV for results.

9. $Fe_2Fv(Tol)_2$ (11). A 0.1-g sample of $(Fe_2Fv(Tol)_2)^{2+}(PF_6^-)_2$ (**4**) (0.14 mmol) in 5 mL of THF is stirred with 10 equiv of Na/Hg amalgam for 3 h at −20 °C under argon. The deep green solution is then transferred to an ESR tube at −80 °C. The same procedure is used for $Fe_2Fv(EtBz)_2$ (**19**), $Fe_2Fv(Mes)_2$ (**20**), and $Fe_2Fv(Bz)(HMB)$ (**21**): see Table I for results.

10. Chemical Characterization of the Complexes $Fe_2Fv(Ar)_2$ (Ar = Bz, Tol, EtBz, Mes, HMB). (a) General Procedure for the Titration by O_2. A 0.058-g sample of $(Fe_2Fv(Bz)_2)^{2+}(PF_6^-)_2$ (0.0845 mmol) is stirred in 10 mL of THF with 10 equiv of Na/Hg amalgam (1%, 1.676 g) for 2 h at −18 °C, under argon. The THF solution is then filtered at −80 °C into another Schlenk tube. Dioxygen (0.475 mL, $^1/_4$ equiv, 0.0211 mmol) is first added; the green color of the solution instantaneously disappears; a purple precipitate of the known complex $(Fe_2Fv(Bz)_2)^+(PF_6^-)$ and $^1/_2$ equiv of Na_2O_2 are formed. Further reaction with 1/4 equiv (0.0211 mmol) of O_2 gives, in 30 mn, the orange solid $(Fe_2Fv(Bz)_2)^{2+}(PF_6^-)_2$ (0.052 g, 0.0761 mmol, 90% yield), identified by comparison with an authentic sample.

The same titration applied to $Fe_2Fv(Tol)_2$, $Fe_2Fv(Mes)_2$, $Fe_2Fv(HMB)_2$, $Fe_2Fv(EtBz)_2$, and $Fe_2Fv(Bz)(HMB)$ gives equivalent results and yields in dicationic species.

(b) General Procedure for the Titration by I_2. A 0.060-g sample of $(Fe_2Fv(Bz)_2)^{2+}(PF_6^-)_2$ (0.0874 mmol) is stirred in 10 mL of THF with 10 equiv of Na/Hg amalgam (1%, 1.7 g) for 2 h at −18 °C under argon. The green THF solution is then filtered at −80 °C in another Schlenk tube; 22 mg (0.0874 mmol) of I_2 are dissolved in 50 mL of THF, and half of the volume is added to the THF solution of **17**. The green solution immediately turns purple, and a purple precipitate of $(Fe_2Fv(Bz)_2)^+PF_6^-$ and NaI (1 equiv) forms. The remaining solution of I_2 is added, and the oxidation is complete in 30 min leading to an orange solid identified by ^1H NMR as $(Fe_2Fv(Bz)_2)^{2+}(PF_6^-)_2$ (0.055 g, 0.0804 mmol, 92% yield). NaI (0.024 g, 92%) was also recovered. The same titration applied to the other $Fe^{I}Fe^{I}$ complexes gives similar results and yields.

Scheme I[a]

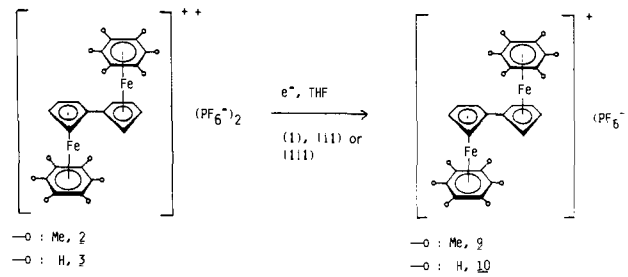

[a] (i) Na/Hg, 20 °C (—o = Me) or −20 °C (—o = H); (ii) $LiAlH_4$ (−80 °C; all cases; (iii) FeCp(HMB), 20 °C (—o = Me) or −20 °C (—o = H).

Scheme II

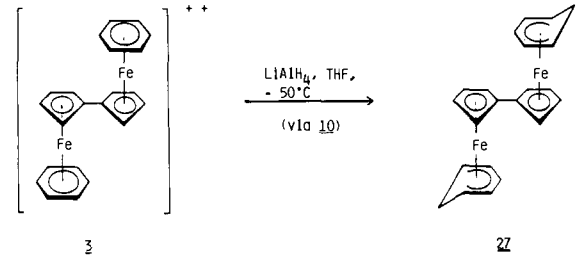

11. $Fe_2Fv(C_6Et_6)_2$ (22). The same procedure as in preparation 8 was used to obtain **22**: see Table IV for results.

12. $Fe_2Fv(C_6H_7)_2$ (27). A 0.1-g sample of complex **3** (0.145 mmol) in 10 mL of THF is stirred with 0.277 g of $LiAlH_4$ (7.288 mmol) for 30 min at −50 °C. THF is then concentrated, and a large excess of toluene is added. The orange solution is filtered, concentrated, and cooled down at −80 °C overnight. Hydrogenated complex **27** (8 mg, 14%) is obtained as pure product: ^1H NMR (C_6D_6, 20 °C) δ 5.83 (m, H_p, 1 H), 4.33 and 4.06 (m, Fv, 8 H), 3.93 (m, H_m, 4 H), 2.50 to 1.50 (m, H_o, H_{endo}, H_{exo}, 8 H).

Results

Delocalized Mixed-Valence $Fe^{I}Fe^{II}$ Complexes. Syntheses and Reactivity. The mixed-valence $Fe^{I}Fe^{II}$ cation **9** is synthesized at 20 °C by Na/Hg reduction of the dication **2** in THF in 2 h. This thermally stable purple complex gave satisfactory elemental analysis confirming its molecular structure. It is, however, only moderately stable at 20 °C in acetone and acetonitrile and has to be handled in these polar solvents at low temperature. The parent analogues **10–15** are obtained similarly but at −20 °C because of their thermal instability and tendency to dimerize. All the complexes **9–15** can also be generated in THF using either 1 equiv of FeCp(HMB), **25**, at 20 °C for **9** and **15** and −20 °C for **10–14** or excess $LiAlH_4$ (100/1) at −80 °C[14] (Scheme I).

Low-temperature reactions are required to obtain **9–15** using $LiAlH_4$ in THF. Single ET proceeds but not the second one.

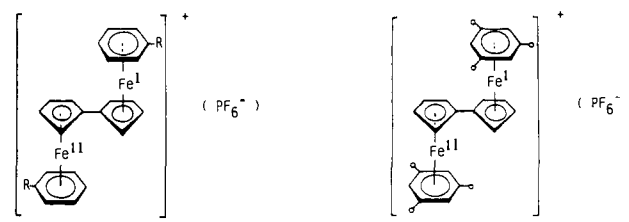

$(Fe_2Fv(Bz)_2)^+(PF_6^-)$, **10** (R = H).
$(Fe_2Fv(Tol)_2)^+(PF_6^-)$, **11** (R = Me).
$(Fe_2Fv(EtBz)_2)^+(PF_6^-)$, **12** (R = Et).
$(Fe_2Fv(Mes)_2)^+(PF_6^-)$, **13**.

Instead, above −50 °C, H atom transfer occurs from the hydride onto the arene ligand, which provides ferrocene-like bis-cyclohexadienyl compounds[14] (Scheme II).

(14) Michaud, P.; Astruc, D.; Ammeter, J. H. *J. Am. Chem. Soc.* **1982**, *104*, 3755. See also ref 6b.

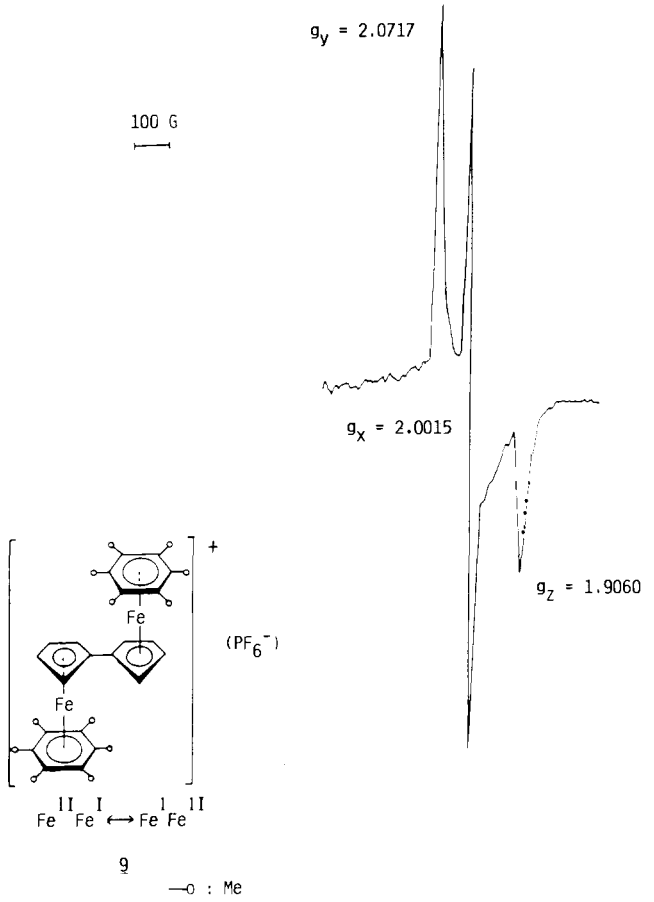

Figure 1. ESR spectrum of $(Fe_2Fv(HMB)_2)^+PF_6^-$, in frozen THF solution (3×10^{-4} mol/L) at 77 K.

For example, the orange complex **27** is formed via **10** from **3** by a succession of ET and H atom transfers provided the reaction temperature does not overtake −50 °C. We already know that hydride reaction with iron–arene cationic Fe^{II} proceeds by the ET mechanism in mononuclear series.[14] The other complexes **11–15** behave similarly. Complex **27** has the same properties as its isomer **28** obtained by slow dimerization of $Fe^{I}Cp(C_6H_6)$ **26**.

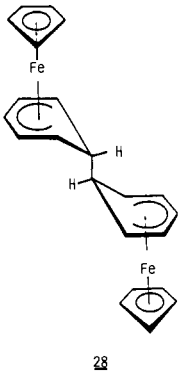

28

Upon contact with air or I_2, in the presence of 1 equiv of $NaPF_6$ salt, the purple $Fe^{I}Fe^{II}$ monocations are smoothly transformed into the oxidized $Fe^{II}Fe^{II}$ dications.

Spectroscopic Characterization. All the complexes of the series **9–15** generated from **2–8** and $LiAlH_4$ or 1 equiv of FeCp(HMB) show by ESR spectroscopy three anisotropic *g* values close to 2 (frozen THF solutions, 77 K), as the Fe^{I} monomers[15] (Table I, Figure 1), which is characteristic of rhombic distortion. The hyperfine couplings are never observed because of fast spin–lattice relaxation. The magnetic susceptibility was determined by the Gouy method for the thermally stable complex **9**. It indicates a Curie–Weiss behavior ($\chi = C/(T + \Theta)$) in the range 70–298 K, close to that expected for the spin-only value, $\mu = 1.7\ \mu_B$.

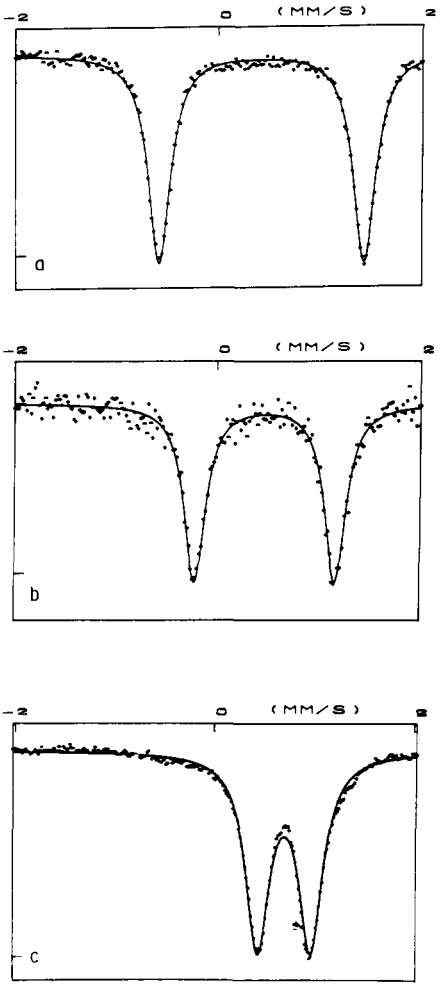

Figure 2. Typical ^{57}Fe Mössbauer spectra of $36e^-$, **2**; delocalized $37e^-$, **9**; and $38e^-$, **16**; complexes with (a) **2** (77 K); (b) **9** (290 K); and (c) **16** (120 K).

The purple color of all the series $Fe^{I}Fe^{II}$ monocations corresponds to an absorption at λ 554 nm with $\epsilon = 7660$ L mol^{-1} cm^{-1} (**9**). This color is at variance with the forest-green color of Fe^{I} monomers[16b] but is not unusual.[5b,c]

The most interesting information is obtained from the Mössbauer spectra with and without applied magnetic field. They were recorded from recrystallized samples of **9** and quickly precipitated samples (−20 °C) of the thermally unstable parent compound **10**.

The $37e^-$ complexes were studied over a broad temperature range. Only one doublet is observed (Figure 2b) in this experimental temperature range; therefore, we conclude that **9** and **10** are delocalized mixed-valence compounds on the Mössbauer time scale (10^7 s^{-1}). The IS values correspond to the average of IS values for Fe^{II} and Fe^{I} of monomers, respectively, at room temperature. Thus, in the $37e^-$ complexes, the electron which is added upon reduction of the $36e^-$ complexes is shared between the two iron centers. The complexes can effectively be considered as $18.5e^-$ systems. The QS turns out to be practically temperature independent, pointing out the larger energy difference between the HOMO and LUMO than in monomeric species and the lack of Jahn–Teller activity, compared to monomers.[16]

(15) Rajasekharan, M. V.; Giezynski, S.; Ammeter, J. H.; Ostwald, N.; Michaud, P.; Hamon, J.-R.; Astruc, D. *J. Am. Chem. Soc.* **1982**, *104*, 2400.

(16) (a) Astruc, D.; Hamon, J.-R.; Althoff, G.; Román, E. Batail, P.; Michaud, P.; Mariot, J.-P.; Varret, F.; Cozak, D. *J. Am. Chem. Soc.* **1979**, *101*, 5445. (b) Hamon, J.-R.; Astruc, D.; Michaud, P. *Ibid.* **1981**, *103*, 758. (c) Astruc, D. Tetrahedron Report No. 157, *Tetrahedron* **1983**, *39*, 4027.

Table II. ^{57}Fe Mössbauer Parameters of FeCp(arene) Monomers and Dimers[a]

compd	no. of electrons	T (K)	IS (mm/s)	QS (mm/s)
24	18	77	0.52	1.64
		rt[c]	0.41	1.64
23	18	77	0.56	2.00
		rt[c]	0.45	2.00
26	19	77	0.87	0.95
		rt[c]	0.74	0.33
25	19	77	0.85	0.56/1.18
		rt[c]	0.74	0.50
3	18 + 18	rt[c]	0.44	1.66
2	18 + 18	77	0.54	2.00
10	18.5 + 18.5	5.5	0.68	1.17
		77	0.66	1.17
		200[b]	0.62	1.16
9	18.5 + 18.5	4.2	0.69	1.35
		77	0.68	1.36
		rt[c]	0.58	1.38
17	19 + 19	110	0.85	0.72
		160[b]	0.81	0.55
16	19 + 19	5	0.81	1.75
		80	0.84	0.62
		290	0.73	0.46
22	19 + 19	4.5	0.84	1.52
		80	0.84	1.38
		200	0.81	1.12
		280	0.77	0.91

[a] IS is relative to α-Fe at room temperature. [b] Unstable at room temperature. [c] rt stands for room temperature.

Table III. Saturation Values of the Hyperfine Field Components Derived from Fitting Magnetic Hyperfine Spectra of **9** (37e$^-$) and for Comparison Corresponding M Results

T (K)	H_x	H_y	H_z	H_{iso}[a]
4.6	−9.4	−0.8	−3.9	−4.7
8	−10.4	−0.9	−4.7	−5.3
18	−12.8	−0.8	−6.8	−6.8
MO[b]	−17.5	−1.1	−3.1	−7.2

[a] $H_{iso} = (H_x + H_z)/3$. [b] MO values derived according to the procedure described in ref 18 and 19.

A 6 T magnetic field has been applied to **9** parallel to the γ-beam, between 4.6 and 200 K. At 200 K the shape of the spectrum results from the combination of the electric field gradient (efg) and the applied field only, because hyperfine contributions are zero due to vanishing spin expectation values at elevated temperature. The spectrum at 200 K (Figure 3a) is nearly symmetric which is typical for a large asymmetry parameter η. The fitted value is $\eta \simeq 0.7$.[17] The main component of the efg is negative. At lower temperature (<18 K), the computed line shape (Figure 3b–d) accounts for a hyperfine field $-A\langle S\rangle$ due to the paramagnetism of the system. Initial values for the hyperfine field tensor were estimated from MO calculations corresponding to the procedure described in ref 17–19. Values for QS and IS have been taken from zero-field spectra (Table II). η and the sign of the main component of efg have been derived from the magnetic 200 K spectrum; all these parameters were kept fixed.

The expectation value $\langle S\rangle$ was calculated from the thermal population of a two-level system with isotropic g value ($g = 2$). The results of the fit are reported in Table III.

The deviation between the values at different temperatures probably arises from the complexity of the spectra, including diamagnetic 18e$^-$ impurities[20] (Figure 3) and from the approximation with which the fit procedure has been carried out, i.e., axes between efg tensor and hyperfine field tensor were kept collinear.

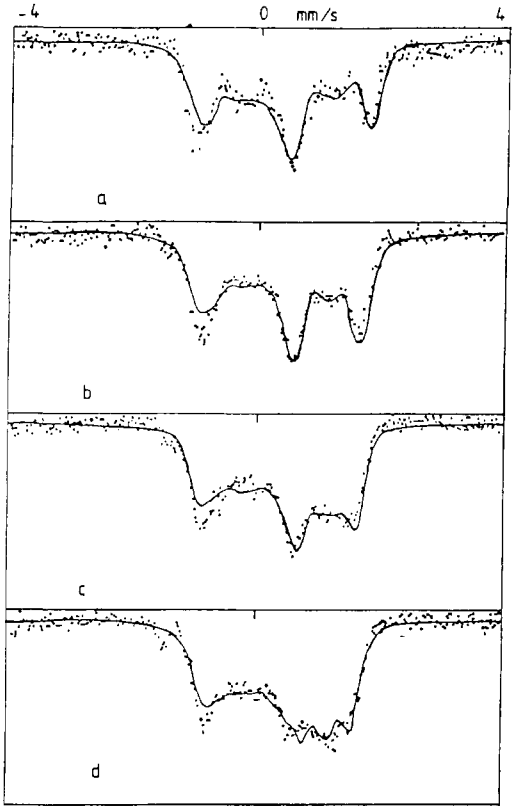

Figure 3. ^{57}Fe Mössbauer spectra for **9** under externally applied magnetic field (H^{ext} = 6 T, parallel to the γ-beam at (a) 200 K, (b) 20 K, (c) 18 K, and (d) 6.3 K. These spectra were obtained from experimental data corrected from a diamagnetic 18e$^-$ impurity, the amount of which was known from a zero-field measurement. Theoretical curves are explained in the text.

Scheme III

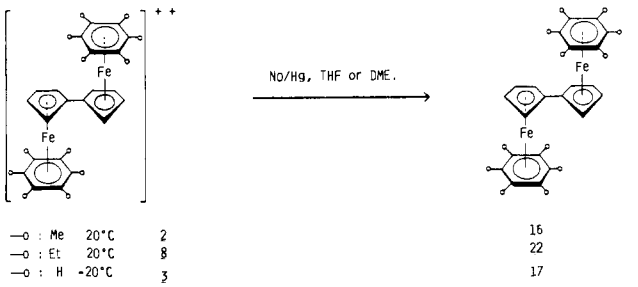

From the Fermi contact term found (−5.5 T), under the magnetic field of 6 T, the electron density per iron corresponds to 42% of the expected contribution of the total spin density of one electron; this depicts the delocalized electron as shared between the two iron centers, with a residue of 16% spin density on the ligands.[18b]

The near-infrared region has been examined in order to locate an intervalence band. An absorption is observed in this region at 989 nm for **9** in acetonitrile solution; however, the low ε value obtained (ε = 170 L mol^{-1} cm^{-1}) does not allow us to attribute this band to an intervalence one. No other absorption has been found in the near-infrared region.

Fe^{I}Fe^{I} Biradicals. Syntheses. The Fe^{II}Fe^{II} dicationic precursors can be reduced by Na/Hg in THF not only to the Fe^{II}Fe^{I} cations but also further to the Fe^{I}Fe^{I} neutral complexes. The mixed-

(17) Varret, F. *J. Phys. Chem. Solids* **1976**, *37*, 265.
(18) (a) Mariot, J.-P.; Guillin, J.; Varret, F.; Lauer, S.; Trautwein, A. X. *Hyperfine Interact.* **1986**, *30*, 221. (b) Guillin, J.; Desbois, M.-H.; Mariot, J.-P.; Lauer, S.; Trautwein, A. X.; Varret, F.; Astruc, D. *Hyperfine Interact.* **1986**, *28*, 761.
(19) Marathe, V. R.; Trautwein, A. X. In *Advances in Mössbauer Spectroscopy*; Elsevier: Amsterdam, 1983; p 398.
(20) Oxidation reactions have been studied in detail and shown to occur at the surface without perturbation of the cooperativity between the molecular distortion and the lattice in Fe^{I} complexes: Astruc, D.; Hamon, J.-R.; Román, E.; Michaud, P. *J. Am. Chem. Soc.* **1981**, *103*, 2431.

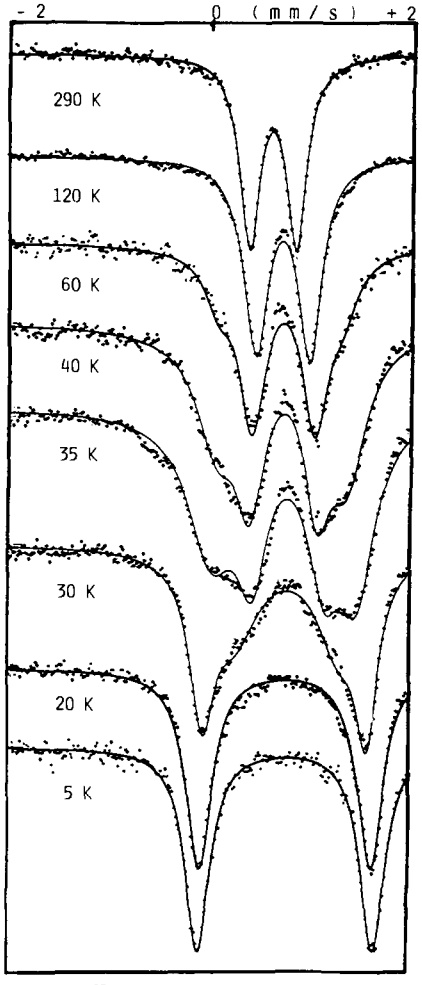

Figure 4. Evolution of ^{57}Fe Mössbauer spectra of the 38e$^-$ Fe^IFe^I complex, **16** with the temperature between 5 and 290 K. Note the phase transition in the range 30–60 K.

valence complexes progressively turn from purple to dark green, the color of the biradicals. The thermally stable, extremely air-sensitive Fe^IFe^I complex **16** is very insoluble in all common solvents. It quickly reduces acetone[21] giving the purple complex **9**. Its synthesis from **2** at 20 °C using clean, freshly prepared 1% Na/Hg, freshly distilled THF, or DME requires 4 h reduction time (Scheme III).

Other Fe^IFe^I biradicals with fewer Me groups can be made by Na/Hg reduction at −20 °C. These reactions proceed more quickly than for the synthesis of **16** because they are effected at less negative reduction potentials. The reduced forms Fe^IFe^I are more soluble than **16**; for instance, **17–21** are toluene soluble.

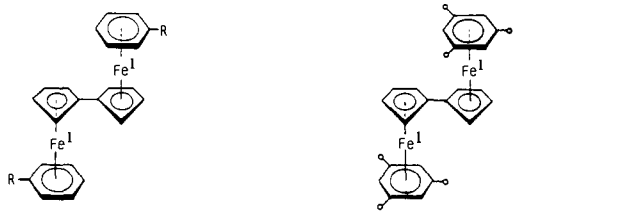

$Fe_2Fv(Bz)_2$, **17** (R = H).
$Fe_2Fv(Tol)_2$, **18** (R = Me).
$Fe_2Fv(EtBz)_2$, **19** (R = Et).
$Fe_2Fv(Mes)_2$, **20**. —o : Me

Electronic Structure. The thermally stable peralkylated complexes **16** and **22** and the thermally unstable parent complex **17** were subjected to Mössbauer spectroscopy. The 4.2 to 220 K spectra of **17** presented, besides the doublet of the Fe^IFe^I system, a few other contributions[20] (36e$^-$, 37e$^-$ complexes and amorphous iron oxide due to decomplexation). This was not the case for Mössbauer samples of **16** which were cleaner and did not contain extra contributions (Figure 4 and Table IV).

(21) The monomer **22** also reduces ketones in refluxing THF more slowly than does the biradical **20**.[3b]

Table IV. Typical ^{57}Fe Mössbauer Data for the 38e$^-$ Complex **16**[a]

T (K)	IS (mm/s)	QS (mm/s)	Γ^b (mm/s)	%
5	0.809 (1)	1.745 (2)	0.296 (4)	100
20	0.812 (1)	1.709 (2)	0.316 (4)	100
30	0.813 (2)	1.640 (5)	0.290 (1)	60
	0.843 (5)	1.020 (2)	0.55 (2)	40
35	0.810 (1)	1.460 (1)	0.450 (2)	49
	0.860 (1)	0.750 (1)	0.430 (1)	51
40	0.819 (4)	1.320 (2)	0.460 (2)	50
	0.845 (3)	0.680 (1)	0.360 (1)	50
60	0.824 (7)	1.110 (6)	0.460 (4)	37
	0.840 (2)	0.600 (1)	0.300 (1)	63
80	0.838 (1)	0.623 (2)	0.298 (3)	100
120	0.821 (1)	0.537 (2)	0.290 (3)	100
290	0.728 (1)	0.465 (2)	0.240 (2)	100

[a] Isomer shifts are relative to α-Fe at room temperature; numbers in brackets are rms deviations of statistical origin. [b] Γ is half the full width at half height of Lorentzian fitting program.

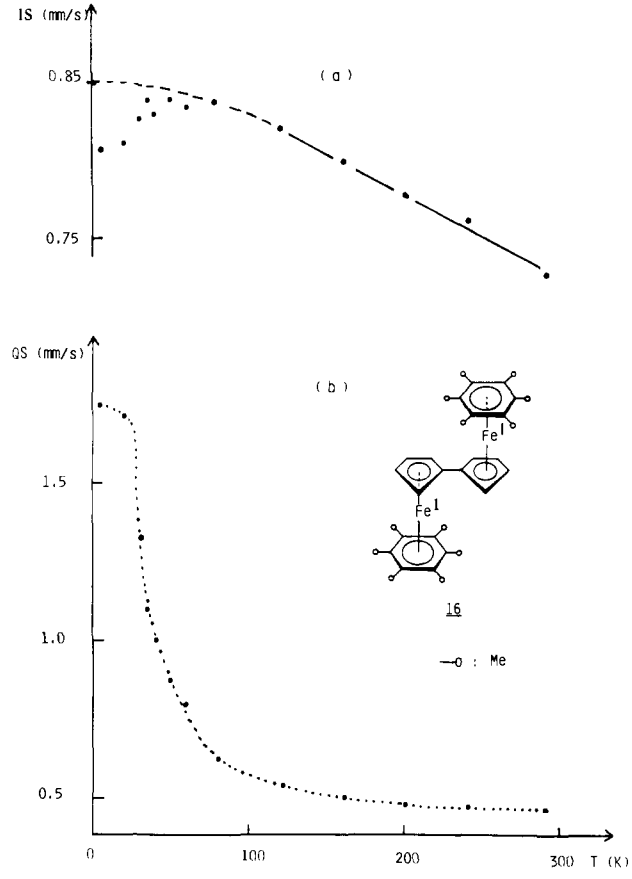

Figure 5. Temperature dependence of (a) the isomer shift (IS) and (b) the quadrupole splitting (QS) for the 38e$^-$ complex, **16**, showing anomalous decrease of IS at low temperature. The line drawn for IS schematizes the usual thermal effect due to second order Doppler shift.

Spectra recorded between 4.2 and 290 K show typical parameters of 19e$^-$ d^7 Fe^I systems (Figure 5); i.e., large IS and temperature dependence of QS. Results obtained for **17** and **22** are summarized in Table II and shown in Figure 6.

The temperature dependence of QS is qualitatively similar to that found for monomers for both complexes **17** and **22**. It follows the regular law observed for Fe^I systems when no coupling between the Jahn–Teller distortion and the lattice occurs (Figure 6). Such a behavior is indicative of disorder in the solid state. Detailed Mössbauer studies of **16** show a significant decrease of IS at low temperature suggesting a phase transition with a decrease of 3d

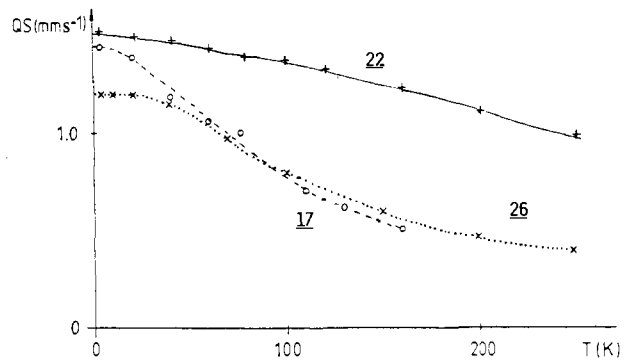

Figure 6. Temperature dependence of the QS for the 38e⁻ complex **17** (o, – –), the corresponding monomeric 19e⁻ complex **26** (x, ···), and the 38e⁻ complex **22** (+, —).

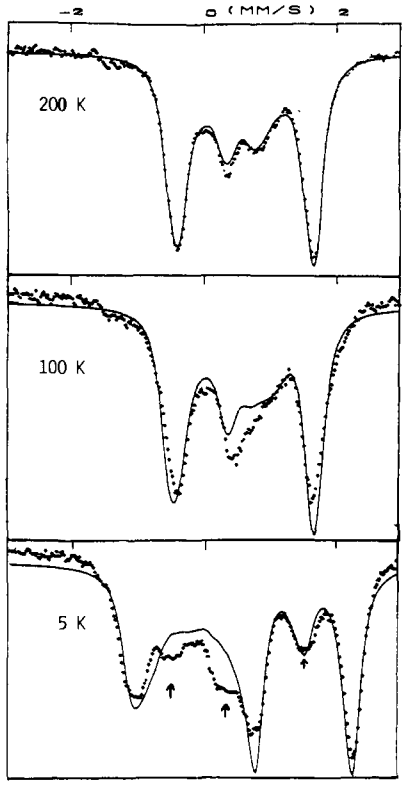

Figure 7. ^{57}Fe Mössbauer spectra of **16** under applied external field of 6 T showing (a) a negative electric field gradient at high temperature (200 and 100 K) and (b) at 5 K, fit in a diamagnetic model ($H_{hyp} = 0$) is consistent with antiferromagnetic coupling of the spins $^1/_2$. Extra lines (arrows) reveal a moderate contribution of the high-temperature phase.

electron density on metals, i.e., with a partial transfer of the extra-electronic density (≃20%) on the fulvalene ligand. It is concomitant with an antiferromagnetic coupling of the two iron spins at low temperature, responsible for the diamagnetic pattern of **16** in the Mössbauer spectra under magnetic field (6 T, negligable magnetic components), (Figure 7) as well as for the decrease of magnetization below 40 K.

However, if the spin up–spin down coupling is important, the electron transfer is not strong enough to be able to chemically couple the two molecular units; this is further supported by the MO results discussed below. These Fe^IFe^I complexes all have a deep green color as Fe^ICp(arene) monomers. The visible spectrum of **17** in toluene at −50 °C, for example, shows an absorption at λ = 725 nm, with ϵ = 1400 L mol^{-1} cm^{-1}. These values analogous to those obtained for Fe^ICp(arene) monomers were attributed to a forbidden $e^*_1 \rightarrow e_2$(arene) transition.[16] Another significant spectroscopic perturbation due to the presence of two anchored Fe^ICp(arene) units is found in the ESR spectra. The latter were recorded for all Fe^IFe^I complexes of these series (**16–22**) in frozen

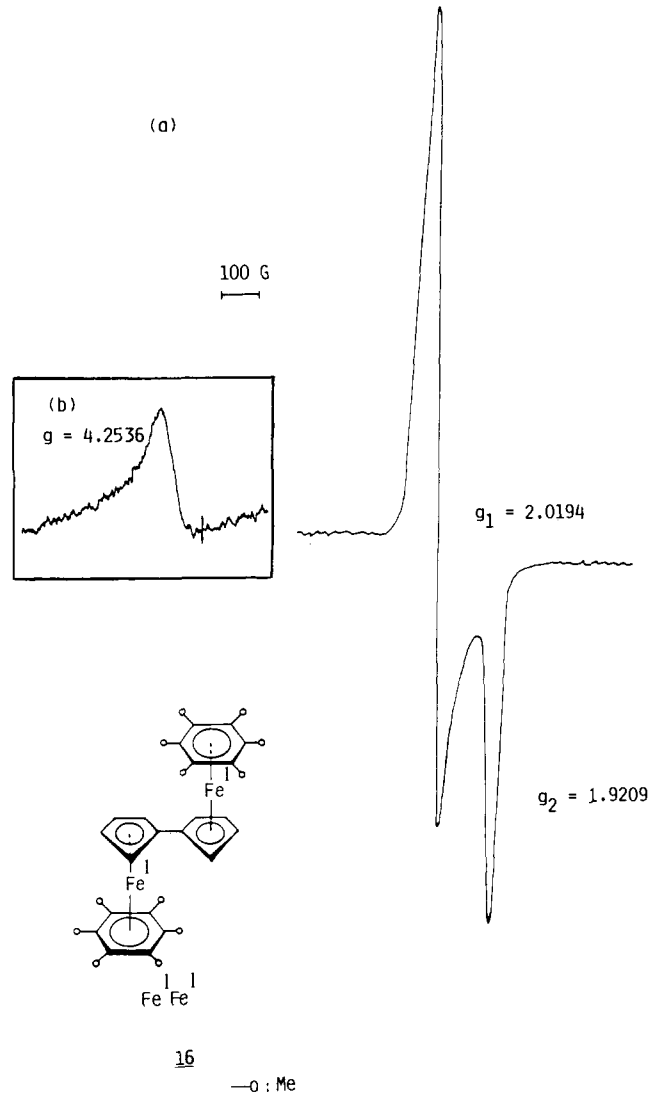

16

Figure 8. ESR spectra of $Fe_2Fv(HMB)_2$, **16**: (a) frozen THF solution (3×10^{-4} mol/L) at 77 K and (b) half-field line in solid state sample.

THF solutions at 77 or 4.2 K or on solid samples (whenever possible) and show two lines around g = 2, whereas the Fe^I monomers and the mixed-valence Fe^IFe^{II} complexes show three g values.[13] One of the two lines is slightly broadened, and their order changes in **20**, the complex in which the steric inhibition of rotation about the Cp–Cp bond is maximum. This change in ESR spectra of Fe^IFe^I is related to the magnetic coupling (dipole + exchange) between the two Fe^I centers. Further interpretation should follow after systematic investigation of the hyperfine couplings; so far it is subjected to caution since the g values in all the Fe^I complexes are extremely sensitive to the host lattice in these dynamic Jahn–Teller systems.[15] Importantly, this ESR activity confirms that the neutral diiron complexes are biradicals with d^7d^7 Fe^IFe^I structures (thermal population of the triplet state S = 1) rather than diamagnetic d^8d^8 Fe^0Fe^0 complexes. Another confirmation of this assumption was the presence of an absorption line at half field in ESR spectra of solid samples of **16** (Figure 8) (because of its low intensity, this line could not be observed in frozen solution spectra).

This extra line is characteristic of triplet states and of ΔMs = 2 transitions. Such transitions are usually forbidden in ESR spectroscopy but can nevertheless be observed in triplet state spectra because the energy of interaction between the electron dipoles is comparable to $g\beta H$. Under such conditions, the usual selection rules break down at low fields since the two spin angular momentum vectors are not independently quantized. This transition, indeed, was not found in the ESR spectra of the Fe^IFe^{II} complex. The magnetic moment obtained from the ESR data

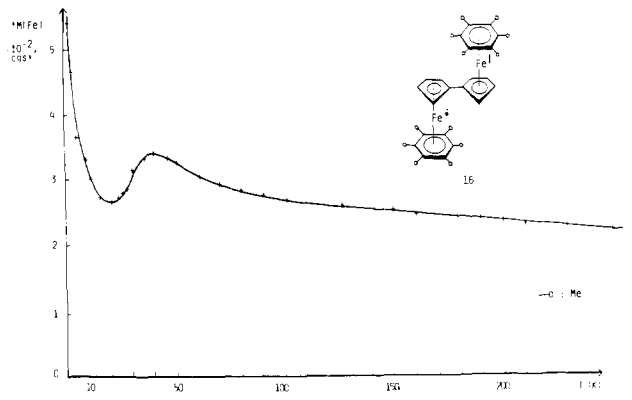

Figure 9. Molar magnetic susceptibility results as a function of the temperature for complex **16**. Molar paramagnetic susceptibilities are corrected for background and for diamagnetism of the compound. Compound diamagnetism is from Pascal's constants and the value is −337 cgsu/mol.

provides values of g between 2.81 and 2.87, in agreement with the theoretical values for triplets ($S = 1$) without significant spin-orbit contribution (eq 1).

$$\mu = (1/3(gx^2 + gy^2 + gz^2)S(S + 1))^{1/2} \quad (1)$$

Variable temperature magnetic susceptibility data were collected between 1.9 and 266 K for the stable, isolable $Fe^{I}Fe^{I}$ complex **20**. The molar magnetic susceptibility (χ_M) vs temperature curve is presented in Figure 12, and experimental data are given in the Supplementary Material. At first sight, this curve seems to be that of an antiferromagnetic compound containing a certain amount of isolated paramagnetic impurity. Above 20 K, the susceptibility consecutively increases and decreases with the temperature, the maximum being given for 37 K (Figure 9).

The extrapolation of the low-temperature region seems to give a zero susceptibility value at 0 K. This behavior is typical of magnetically coupled dimers with an antiferromagnetic intramolecular exchange constant. Assuming the interaction is of the Heisenberg type, the susceptibility follows the Bleaney–Bowers equation[22] (eq 2).

$$\chi = (Ng^2\mu_B^2/3k_BT)(1 + (1/3)\exp(-2J/k_BT))^{-1} \quad (2)$$

This equation assumes that J (magnetic exchange interaction between the two $S_1 = S_2 = 1/2$ centers) is isotropic; i.e., the spin Hamiltonian $H = -2JS_1S_2$ applies. Unfortunately, the susceptibility curve cannot be satisfactorily fitted with such an equation which is not surprising in view of the ESR and Mössbauer results obtained under magnetic field. They indeed show that, besides the absence of hyperfine field at 5 K typical of antiferromagnetic coupling of two spins $1/2$, lines due to the paramagnetic high-temperature phase are still observed. The coexistence of these two kinds of magnetism, the probable temperature dependence of the proportion of the paramagnetic phase, and the absence of quantitative data concerning the relative amounts of each phase prevent any fitting of the experimental magnetic susceptibility curve. Nevertheless, a crude estimation of the intramolecular coupling can be obtained from the maximum of susceptibility (37 K). This leads to a J/k_B value close to 50 K, i.e., of the order of magnitude of kT at the temperature of the experimental ESR spectra (frozen THF solution).

Oxidation. The $Fe^{I}Fe^{I}$ complexes are also characterized by their reactions with O_2 and I_2. Reactions of THF solutions of the $Fe^{I}Fe^{I}$ complexes with $1/4$ mol O_2[23] or $1/2$ mol I_2 in the presence of stoichiometric amounts of $NaPF_6$ (2 equiv) at −80 °C immediately give the purple mixed-valence $Fe^{I}Fe^{II}$ PF_6^- salts and $1/2Na_2O_2$ or NaI. Addition of another equal amount of O_2 or I_2 respectively provides the $Fe^{II}Fe^{II}$ dications as the PF_6^- salts in 0.5 h. These two steps of the reaction indicate that $Fe^{I}Fe^{I}$ complexes can assure two successive monoelectronic transfers. This technique gives accurate titrations of solutions of these $Fe^{I}Fe^{I}$ complexes given the sharp and immediate color change from deep green to light purple (and purple precipitate) and orange precipitate in the last step.

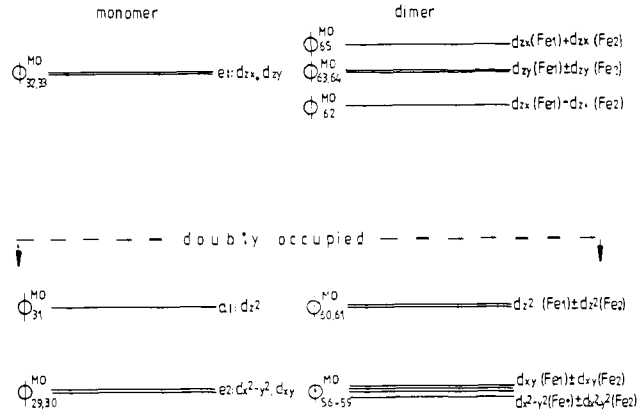

Figure 10. MO diagram of mono- and dinuclear complexes. Only MOs with mainly Fe 3d character are drawn.

Electronic Structure Calculations. We have performed self-consistent charge SCC-Xα molecular orbital (MO) calculations[24] to investigate the electronic structure of the binuclear complexes and to compare these results with those obtained for monomers. Mössbauer parameters have been derived according to the procedure described elsewhere.[18,19,24,25]

Monomers. MO calculations for the monomers ferrocene ($18e^-$), $FeCp(C_6(CH_3)_5CH_2)$ ($18e^-$), $(FeCp(Bz))^+$ **24**, $(FeCp(HMB))^+$ **23**, FeCp(HMB) **25**, and FeCp(Bz) **26** are used as references for comparison with dinuclear complexes. Some of the results are reported in Table V with corresponding values as obtained earlier from Iterative Extended Hückel (IEH) calculations and Mössbauer measurements.[18,25,26]

From these results, we derive the following conclusions: (i) Effective atomic charges q_{at} and atomic orbital (AO) occupation numbers x_{3d} of iron as obtained from the SCC-Xα method are larger than those corresponding to IEH; for AO occupation number x_{4p} the situation is opposite. This is due to the fact that the parametrization of the IEH method yields nearly identical energies for Fe $3d^7$ and Fe $3d^64p^1$ configurations in agreement with Hartree–Fock results of free iron atoms.[30] The parametrization of the SCC-Xα method energetically favors Fe $3d^7$ over Fe $3d^64p^1$ configuration.

(ii) Quadrupole splittings and asymmetry parameters from SCC-Xα are somewhat closer to experimental values than corresponding values from IEH.

(iii) The linear relation between isomer shifts and electron densities according to $\Delta IS = \alpha\Delta\rho(o)$ with α between −0.20 mm s^{-1} a_o^3 and −0.25 mm s^{-1} a_o^3[18,19,25,26] is qualitatively represented by the SCC-Xα values.

Dinuclear Complexes. Since X-ray structures for dinuclear complexes are unknown, MO calculations have been performed on modelized structures (Tables V and VI) with (i) the two identical subunits in trans configuration, (ii) the C–C′ distance being estimated from corresponding biferrocene complexes,[27] and

(22) Bleaney, B.; Bowers, K. D. *Proc. R. Soc. London Ser. A* **1952**, *214*, 451.

(23) Titration of $Fe^{I}Fe^{I}$ complexes with O_2 are effected in the presence of $NaPF_6$ because this salt inhibits the cage reactions (basic or nucleophilic) of $O_2^{\cdot-}$ onto the arene ring of the cation. In this way, only the cations are obtained. For this special salt effect, see: Hamon, J.-R.; Astruc, D. *J. Am. Chem. Soc.* **1983**, *105*, 5951; *Organometallics* **1988**, *7*, 1036.

(24) (a) Grodzicki, M. *J. Phys. B* **1980**, *13*, 2693. (b) Bläs, R. Thesis, Saarbrücken, 1985. (c) Grodzicki, M.; Manning, V.; Trautwein, A. X.; Friedt, J. M. *J. Phys. B*, accepted for publication.

(25) Trautwein, A. X.; Reschke, H.; Deszi, I.; Harris, F. E. *J. Physique* **1976**, *12*, C6-463.

(26) Mariot, J.-P.; Michaud, P.; Lauer, S.; Astruc, D.; Trautwein, A. X.; Varret, F. *J. Phys.* **1983**, *44*, 333.

(iii) the structures for the subunits taken from the corresponding monomers.

MO calculations have been carried out for **3**, **10**, and **17** only (complexes without methyl groups) in order to keep the number of basis AOs small (124 instead of 196, when methyl groups are included).

The calculated energy diagram for **3** exhibits 61 doubly occupied MOs with the HOMO having Fe-3d_{z^2} character (Figure 10). This diagram is completely equivalent to the one of monomer $(FeCp(Bz))^+$. This equivalence continues when comparing effective and calculated charges as well as measured Mössbauer parameters (Tables I, V, and VI). We therefore conclude that **3** is a Fe(II) $18e^- + 18e^-$ complex, with the linkage having little effect on the electronic structure of the two iron sites.

The addition of two electrons to **3** yields **17**, for which we derive qualitatively the same energy diagram as for **3** (Figure 9). Due to this diagram with $\Delta_1 \simeq 1500\ cm^{-1}$, we expect a population of the MO ϕ_{62} with one electron and of the MOs ϕ_{63}, ϕ_{64} with an additional electron yielding a $S = 1$ paramagnetic compound. This is confirmed by the observation that **17** is ESR-active at 77 K. Additionally, the relatively large energy spacings Δ_1 and Δ_2 (Figure 10) which amount to values $\simeq 1500\ cm^{-1}$ are inconsistent with the significant temperature dependence of measured QS (Figure 6). We have found that increasing the C–C′ distance between the two cyclopentadienyl (Cp) rings of **17** from 1.48 to 1.78 Å and then to 2.00 Å drastically decreases the energy spacings Δ_1 and Δ_2. Increasing this distance effectively corresponds to the presence of two weakly coupled $19e^-$ monomers. This situation accounts for the presence of ESR signals as well as for the close similarity of the temperature dependence of QS for **17** and the $19e^-$ monomer **26** (Figure 6). Calculating QS in the "high temperature limit" (Δ_1 and $\Delta_2 \simeq 150\ cm^{-1} \simeq 200$ K, $T = 220$ K) yields a value which is comparable to the measured value (Table VI). Full agreement between calculated and measured T-dependence of QS is obtained when taking into account Jahn–Teller distortion and spin-orbit coupling as described for the monomer **26**.[18,26]

For **10**, MO calculations have been performed with Fe–Cp and Fe–arene distances about halfway between the values used for **3** and **17**. The calculated energy diagram is qualitatively the same as obtained for **3** and **17** (Figure 10). The electronic configuration of the $37e^-$ complex with 61 doubly occupied MOs and one singly occupied MO (ϕ_{62}) is consistent (i) with the observation that this compound is ESR-active[13,16] and (ii) with the calculated effective charges and orbital occupancies for the two iron sites which are between the corresponding values of the $36e^-$ and $38e^-$ dinuclear complexes **3** and **17**, respectively (Table VI). The measured IS and the calculated charge density $\rho(o)$ follow this trend. QS of **10**, however, does not follow this linear interpolation scheme, because it depends on the efg tensor, the various contributions of which are summarized in Table VII. The closed-shell contribution to the efg at each iron site in **10** corresponds to the situation in $(FeCp(Bz))^+$ or **3**. The open-shell contribution from the singly occupied MO ϕ_{62} arises from effectively 0.5 electron with d_{zx} (Fe_1) and 0.5 electron with d_{zx} (Fe_2) character (Figure 10). The resulting total efg components of **10** (Table VII) yield sign of efg, η, and QS, which qualitatively agree with the measured data (Table VI). Additionally, the lacking temperature dependence of QS_{exp} is reflected by the relatively large energy spacings Δ_1 and Δ_2 ($\simeq 1500\ cm^{-1}$) which result from the MO calculations of **10**. These energies would be practically zero, if the Cp–Cp rings were uncoupled, as in the case of **17**. From our findings, we conclude that the $37e^-$ dimer **10** is (i) a delocalized mixed-valence compound with an electron being equally distributed over the two subunits yielding formally a $(18.5 + 18.5)\ e^-$ dimer and (ii) with considerably stronger Cp–Cp coupling than in **17**.

Discussion

The electronic structure of the Fe^IFe^I biradicals is represented by a MO diagram which is definitively at variance with the one

Table V. Calculated Effective Atomic Charges q_{at} and Orbital Occupation Numbers x_{4s}, x_{4p}, and x_{3d} of Iron, Calculated Quadrupole Splittings (QS), Asymmetry Parameters (η), and Isomer Shifts (IS) for Various Monomers Derived from IEH and SCC-Xα MO Calculations (Compare with Experimental QS and IS Data Obtained from Mössbauer Measurements)

method	ferrocene {0[a,b]}		$CpFeC_6(CH_3)_5CH_2$ {0[b]}		24 {0[b,h]}		23 {0[c,h]}		26 {1[d,h]}		25 {1[h]}	
q_{at} in e_o	0.16	(0.91)	0.13	(0.87)	(0.82)		0.26	(0.70)	(0.74)		0.12	(0.54)
x_{4s}[e]	0.20	(0.10)	0.19	(0.10)	(0.09)		0.18	(0.10)	(0.10)		0.18	(0.10)
x_{4p}[e]	1.34	(0.14)	1.16	(0.13)	(0.14)		1.10	(0.15)	(0.09)		1.06	(0.11)
x_{3d}[e]	6.48	(6.85)	6.65	(6.91)	(6.95)		6.50	(7.05)	(7.08)		6.83	(7.25)
QS (mm s^{-1})	+2.85	(+2.42)	[2.40][f]	+2.61 (+2.29)	[+1.89][f]	(+2.26)	[+1.64][f]	+2.59 (+2.40)	[+2.00][f]	[−1.20][h] (+0.85)[g]	[±0.33][i]	[−1.60][h] 1.27[g] (+1.10)[g] [+0.50][i]
η	0	(0)	[0]	0.57 (0.43)	[0.40]	(0)	[0]	0 (0)	[0.10]			
IS[j] (mm s^{-1})			[0.45]		[0.45]		[0.41]		[0.45]	[0.74]		[0.74]
$\rho^*(o)$[k] (a_o^{-3})	67.56	(64.84)	66.91	(64.84)		(64.70)		67.22 (64.50)		(64.00)	65.64	(63.87)

[a] IEH and exp results taken from ref 18, 25, and 26. [b] Structure not known; d(Fe–arene) = 1.53 Å and d(Fe–Cp) = 1.66 Å were taken for calculations. [c] Structure not known; d(Fe–arene) = 1.55 Å and d(Fe–Cp) = 1.68 Å were taken for calculations. [d] Structure not known; d(Fe–Arene) = 1.58 Å and d(Fe–Cp) = 1.78 Å were taken for calculations. [e] Derived from a bond order weighted population analysis.[24] [f] Temperature independent between 4.2 and 300 K. [g] Derived from the simple picture of equally populating the highest occupied MO (HOMO) e_1 (d_{zx}, d_{zy}), i.e., Jahn–Teller distortion and spin-orbit coupling are neglected; full agreement between measured and calculated T dependence of quadrupole splitting is obtained when taking into account Jahn–Teller distortion and spin-orbit coupling within e_1.[18,26] [h] Measured at 4.2 K. [i] Measured at 300 K. [j] Values obtained at 300 K, given relative to α-Fe at 300 K. [k] $\rho(o) = 15000 + \rho^*(o)$; changes of isomer shifts IS may be compared with changes of electron charge densities ($\Delta\rho(o)$) by the relation $\Delta IS = \alpha\Delta\rho(o)$ with $\alpha = -((0.22 \pm 0.03)\ mm\ s^{-1} a_o^3)$.[18,19,25,26] [l] Excess/$18e^-$.

(27) Katuski, Z. *Bull. Acad. Polon. Sci.* **1964**, *XII*, 873.

Table VI. Calculated Effective Atomic Charges q_{at} and Orbital Occupation Numbers x_{4s}, x_{4p}, and x_{3d} of Iron, Calculated QS, Asymmetry Parameters η, and IS for Various Dimers **3**, **10** and **17**, Derived from SCC-Xα MO Calculations (Compare with Experimental QS, η, and IS Data Obtained from Mössbauer Measurements)

compd	**3**[a]	**10**[b]	**17**[c]
excess/36e⁻	0	1	2
q_{at}(Fe)in e_o	0.83	0.78	0.74
x_{4s}[d]	0.09	0.09	0.09
x_{4p}[d]	0.14	0.11	0.09
x_{3d}[d]	6.94	7.01	7.07
QS_{exp} (mm s^{-1})	+1.66[e]	−1.16 (−1.38)[f]	0.55[g]
QS_{calcd} (mm s^{-1})	+2.40[h]	−2.10[i]	+0.89[j]
η_{exp}		0.7[f]	
η_{calcd}	0.0	0.87[i]	0.0
IS (mm s^{-1})	0.44[k]	0.62[l]	0.80[m]
$\rho^*(o)(a_o^{-3})$	64.72	64.35	64.01

[a] Structure not known; d(Fe–arene) = 1.53 Å and d(Fe–Cp) = 1.66 Å were taken for calculations. The C–C′ distance is taken as 1.48 Å, increasing this distance to 1.58 Å practically does not change the calculated orbital occupancies and Mössbauer parameters. [b] Structure not known; d(Fe–arene) = 1.56 Å and d(Fe–Cp) = 1.71 Å were chosen; these values are about halfway between the corresponding values of 18e⁻ and 19e⁻ compounds, respectively. The C–C′ distance is taken as 1.48 Å. [c] Structure not known; d(Fe–Arene) = 1.58 Å and d(Fe–Cp) = 1.78 Å were taken. The C–C′ distance is taken as 1.48 Å; increasing this distance to 1.78 Å practically does not change calculated orbital occupancies and Mössbauer parameters; however, it reduces the energy spacings Δ_1 and Δ_2 (Figure 10) drastically. [d] Derived from a bond order weighted population analysis.[24] [e] Measured at room temperature; sign and temperature independence of efg are assumed to be as in the corresponding monomer **31**. [f] Temperature independent between 5.5 and 200 K; sign of efg and asymmetry parameter η are assumed to be the same as in 9, the value of which is given in brackets. [g] Measured at 220 K, where the high temperature limit of QS has been reached (Figure 6). [h] Value derived from doubly occupied MOs $\phi_1 \cdots \phi_{61}$ (Figure 10). [i] Value derived from doubly occupied $\phi_1 \cdots \phi_{61}$ and singly occupied HOMO ϕ_{62} (Figure 9); due to the relatively large enegy gap $\Delta_1 \simeq$ 2000 K the calculated QS and η are temperature independent. [j] Value derived from doubly occupied $\phi_1 \cdots \phi_{61}$ and from the MOs ϕ_{62} to ϕ_{65} (Figure 10); each of them being occupied by 0.5 electron. This situation corresponds to the high temperature limit with small energy spacings Δ_1 and $\Delta_2 \simeq$ 200 K and T = 220 K. [k] Measured at room temperature, relative to α-Fe at 300 K. [l] Measured at 200 K, relative to α-Fe at 300 K. [m] Measured at 220 K, relative to α-Fe at 300 K. [n] $\rho(o)$ = 1500 + $\rho^*(o)$; derived from the same electronic configuration from which QW_{calcd} has been obtained; changes of isomer shifts (ΔIS) may be compared with changes of electron charge densities ($\Delta\rho(o)$) by the relation $\Delta IS = \alpha\Delta\rho(o)$ with $\alpha = -((0.22 \pm 0.03)$ mm $s^{-1}a_o^3)$.[18,19,25,26]

Table VII. Calculated Values (in mm s^{-1}) of the Main Components of the efg Tensor for **10**

	V_{xx}[d]	V_{yy}[d]	V_{zz}[d]
closed shell[a]	−1.13	−1.13	+2.26
open shell[b]	−0.75	+1.25	−0.50
total[c]	−1.88	0.12	+1.76

[a] Value corresponding to **24**. [b] Derived from MO ϕ_{62} only. [c] The symmetry parameter η is derived from the total efg components, i.e., $\eta = |V_{yy} - V_{zz}|/|V_{xx}|$; the sign of the efg corresponds to the sign of V_{xx}. [d] The main axes system of the efg practically coincides with the molecular axes system.

needed to explain that of the mixed-valence 37e⁻ complexes. The latter needs maximum conjugation between the two sandwich units, i.e., both Cp rings of the Fv ligand in the same plane in order to transfer the extra electron between the two iron centers (which have high spin densities). Given the bulk of the two arene ligands, the electron jump must indeed proceed efficiently through a planar fulvalene ligand. If this were the case in the biradicals, strong coupling between the two sandwich units would be observed. Instead, the two Fe^I sandwich units are found to be relatively independent from each other in the high phase temperature since the Mössbauer and visible spectra are similar to those of Fe^I monomers.[16] At low temperature, sizable spectroscopic differences are found in (i) the perturbed ESR spectra, (ii) the Mössbauer data obtained under external field, and (iii) the magnetic susceptibility curve which all show an antiferromagnetic coupling. Thus chemical coupling to 36e⁻ Fe^0Fe^0 fulvalene does not occur; only magnetic interaction is observed. This can be understood on the basis of a free rotation about the single Cp–Cp bond which impedes π overlap. At this time, the MO diagram is as that of the Fe^I monomers with Jahn–Teller activity due to the single occupancy of a high metal character MO,[28] whereas the 37e⁻ mixed valences do not include rotation effect. A similar situation was recently reported by Geiger for diphenyl dichromium complexes for which the angle between the two phenyl rings of the diphenyl ligand was found to drop from 50° in the Cr^0Cr^0 complex to 0° in the mixed-valence Cr^0Cr^I one.[29]

Conclusion

1. The reduced states $(Fe_2Fv(Ar)_2)^{n+}$, n = 0, 1 were obtained from the dicationic precursors for various arenes using Na/Hg reduction but are stable only with peralkylated arenes C_6R_6 (R = Me or Et). Reduction with $Fe^ICp(HMB)$ or $LiAlH_4$ gives monoreduction to the 37e⁻ complexes, but the latter reagent ultimately leads to $Fe_2Fv(C_6H_7)_2$ when Ar = C_6H_6. Oxidation of the reduced states with I_2 or O_2 + $NaPF_6$ gives back the dications.

2. The purple 37e⁻ monocations were found, by Mössbauer spectroscopy, to be delocalized mixed-valence Fe^IFe^{II} complexes with 42% spin density on each iron atom (84% on the two Fe's) and no Jahn–Teller activity. EHT and SCC-X molecular orbitals calculations confirm that the HOMO is nondegenerate and that the coupling brings about enough HOMO–LUMO separation to inhibit a thermal population of the latter.

3. The green 38e⁻ Fe^IFe^I complexes behave as metal-centered biradicals at room temperature with a Jahn–Teller activity comparable to that of monomeric Fe^I complexes. This indicates that the two sandwich units are fairly independent at room temperature and that there is a good degree of free rotation about the Cp–Cp bond. The Mössbauer and magnetic susceptibility data show an antiferromagnetic transition around 37 K, coupled with a phase transition (C_6Me_6 complex only).

Acknowledgment. We thank Drs. N. Ardoin, F. Moulines, F. Van Gastel, and M. Lacoste (Laboratoire de Chimie Organique et Organométallique, Université de Bordeaux I) for experimental help, Dr. J.-J. Girerd (Laboratoire de Spectrochimie des Elêments de Transition, Université de Paris-Sud, Orsay), Dr. B. Nickel, M. A. Jeunet (LEEDS, Université de Grenoble, Saint-Martin d'Here), E. Marquestaut, and Dr. J.-M. Dance (Laboratoire de Chimie du Solide du CNRS, Université de Bordeaux I) for valuable ESR assistance, and Dr. R. Chevrel and M. G. Jegadin (Laboratoire de Chimie du Solide et Inorganique Moléculaire, Université de Rennes I) for preliminary magnetic studies on the mixed-valence series. DGRST grants to M.-H.D. and J.G. in the preliminary stage of the study are acknowledged as well as a 2-year post-doctoral grant from the Humboldt foundation to J.G. at Lübeck. The excellent collaboration of Dr. J.-P. Mariot (Le Mans) was greatly appreciated in the preliminary stages of the Mössbauer work. Stimulating discussions with all these scientists and with Dr. J.-R. Hamon (Universite de Rennes) are gratefully acknowledged.

Supplementary Material Available: Table containing variable temperature magnetic susceptibility data for **16** (1 page). Ordering information is given on any current masthead page.

(28) For MO diagrams of d^7 sandwich complexes, see: (a) Anderson, S. E.; Drago, R. S. *Inorg. Chem.* **1972**, *11*, 1564. (b) Anderson, S. E.; Rai, R. *Chem. Phys.* **1970**, *92*, 4831. (c) Warren, K. D. *Struct. Bond.* **1976**, *27*, 45. (d) Clack, D. W.; Warren, K. D. *Ibid.* **1980**, *39*, 1.

(29) Van Order, N.; Geiger, W. E., Jr.; Bitterwolf, T. E.; Rheingold, A. L. *J. Am. Chem. Soc.* **1987**, *109*, 5680.